

Domain-wall dynamic transitions in thin films

Samuel W. Yuan*

Department of Physics, University of California, San Diego, La Jolla, California 92093

H. Neal Bertram*

Department of Electrical and Computer Engineering, University of California, San Diego, La Jolla, California 92093

(Received 30 April 1991; revised manuscript received 12 July 1991)

Two-dimensional domain-wall configurations and dynamics in thin films with the easy axis parallel to the film plane are calculated by using LaBonte-like energy minimization as well as solving the Landau-Lifshitz equation with phenomenological damping. Under a sufficiently small uniform field applied in the easy direction, the effective wall mass and the viscosity coefficient induced from a uniform wall motion are compared with theoretical values. For external fields much greater than the anisotropy field, the wall motion exhibits complex features, including periodic transitions between asymmetric Bloch and Néel wall structures and the emergence of multivortices, depending on the film thickness. The latter serves as a precursor to turbulent wall dynamics at even higher external fields. With a varying external field applied in the hard direction and parallel to the film surface, wall structure changes between asymmetric Bloch- and Néel-type walls are also seen. An irreversible transition is observed which causes a constricted hard-axis hysteresis loop. Dynamically, this hysteretic transition can be associated with wall creep.

I. INTRODUCTION

The structure and dynamics of domains and domain walls in ferromagnetic materials have long been a subject of intense study. Although the properties of domain walls in bulk material are well understood by one-dimensional micromagnetics,¹⁻³ complications of magnetostatic interactions arise in films of finite thickness. For extremely thin films, a Néel wall is the stable wall configuration, whereas in thick films, a Bloch wall is energetically more favorable, mainly due to the magnetostatic contributions from the film surfaces.⁴ For infinitely thick films, the classical Bloch wall in bulk material is recovered. However, for Permalloy thin films within the intermediate thickness range of hundreds to thousands of angstroms, a flux closure, single vortex wall occurs,⁵⁻⁹ also referred to as an asymmetric Bloch wall. That a domain wall in thin films has such a two-dimensional structure has been since confirmed experimentally.¹⁰⁻¹³

Although much attention has been given to the static structure of the equilibrium two-dimensional wall recently^{13,14} and a very good understanding has been obtained, only approximate studies of the dynamic properties of these asymmetric Bloch walls have been undertaken.^{15,16} Also, in studying wall motion in thin films,¹⁷⁻¹⁹ it was noticed that the transition from Bloch- to Néel-like walls under an applied field in the hard direction greatly changes the wall dynamics. It is our effort here to present quantitative results from micromagnetic numerical modeling of two-dimensional wall structure and dynamics.

II. EQUILIBRIUM WALL STRUCTURES

The configuration we studied is similar to LaBonte,⁵ where the easy axis lies in the film plane, and the discreti-

zation region is in the cross section normal to the film plane (Fig. 1). To find the equilibrium wall configurations, the minimization of energy requires that \mathbf{M} must be parallel to \mathbf{H}_{eff} (Ref. 20) inside the domain as well as the wall region. The effective field is the variational derivative of the energy density:

$$\mathbf{H}_{\text{eff}} = - \frac{\partial \epsilon}{\partial \mathbf{M}} . \quad (1)$$

Using the Cartesian coordinate system depicted in Fig. 1, the total energy density of the domain wall can be written as follows, consisting of contributions from exchange, uniaxial anisotropy, magnetostatic, and Zeeman energy, respectively,

$$\epsilon = \frac{A}{M_s^2} |\nabla \mathbf{M}|^2 - \frac{K}{M_s^2} M_z^2 - \frac{1}{2} \mathbf{H}_D \cdot \mathbf{M} - \mathbf{H}_0 \cdot \mathbf{M} , \quad (2)$$

where A is the exchange constant, K is the crystalline uniaxial anisotropy constant, M_s is the value of saturation magnetization, and \mathbf{H}_D and \mathbf{H}_0 are the demagnetization field and the external field, respectively. For the magnetostatic energy, an expression slightly different from those proposed previously^{5,13,21,22} is adopted; here a simple form of the two-dimensional magnetostatic interaction field matrix has been utilized (Appendix A). This long-range interaction term dominates the computation time.

Starting from virtually any random initial wall configuration, \mathbf{M} and \mathbf{H} are made parallel iteratively over the entire discretization region; this procedure is terminated once the maximum change of the magnetization component from successive iterations reaches an error requirement of within 1×10^{-5} . A typical Bloch wall in a 1000-Å-thick Permalloy film is shown in Fig. 1. The asymmetric feature can be clearly seen from the distribu-

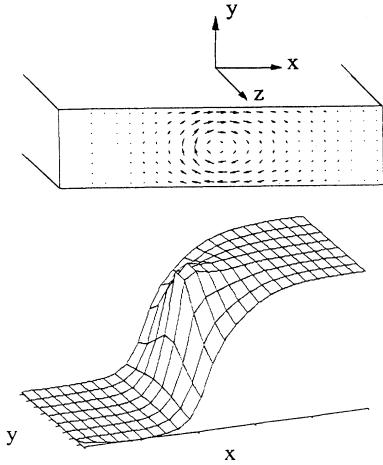


FIG. 1. A typical asymmetric Bloch domain wall in a 1000-Å-thick Permalloy film. Uniaxial crystalline anisotropy easy axis is along z . Film plane is parallel to the x - z plane. Upper graph shows the magnetization vector projections in the x - y plane; lower graph shows the distribution of the z component of magnetizations.

tion of the easy-axis component of magnetizations. This asymmetric Bloch wall consists of Néel-like walls at the film surfaces and Bloch-like wall at the film center. The deviation of the finite-thickness film magnetization profiles from those for the bulk materials comes from the magnetostatic coupling interaction between the two opposite film surfaces, resulting in an energetically favorable flux-closure single vortex.¹³

The material parameters are typical for Permalloy: exchange constant $A = 1.0 \times 10^{-6}$ erg/cm, anisotropy constant $K = 1.0 \times 10^3$ erg cm⁻³, and saturation magnetization $M_s = 800$ emu cm⁻³. Discretization number (N_x, N_y) used ranged from (25,8) to (200,16) with little change in the wall configuration and the final total energy. Excellent agreements have been obtained with previous calculations.⁵ Starting from different initial conditions and following different iteration paths did not change the final result: only the center and the rotation sense (chirality) of the flux-closure vortex may be different.

The vortex structure is mainly due to the presence of magnetostatic interactions in the thin film. Thus it is interesting to see how this structure is affected by the mag-

nitude of the saturation magnetization. Table I gives a list of the wall energies of a 1000-Å-thick film at various magnetizations. A necessary condition for the final equilibrium to be a true minimum-energy state is that the self-consistency parameter proposed by Aharoni²³ is close to one. In Table I it is seen that this is well satisfied. The requirement of S being close to unity is also met by all of our other energy-minimization results as well. As the magnetization increases, so does the total wall energy. In Fig. 2 this trend is compared with a simple one-dimensional variational approximation.²⁴ This 1D prediction only shows a qualitative trend rather than a quantitative result. By comparing the energy, it is seen that a 1D Néel wall is more favorable than a Bloch wall at small saturation magnetization values. A similar result is certainly obtained by our two-dimensional simulations. From the magnetostatic energy in Table I, one can see that the flux-closing vortex structure is most favorable at an optimum magnetization. For $M_s \geq 300$ emu cm⁻³, virtually only a vortex wall exists; for $M_s = 200$ emu cm⁻³, however, a Néel wall occurs (Fig. 3). In this case, the magnetization reverses its direction along the x direction over a distance larger than the film thickness, hence the exchange energy is reduced compared to the vortex wall, where the magnetization reverses direction across the film thickness; the magnetization divergence in the Néel wall replaces the flux closure in the vortex wall, hence the magnetostatic energy is increased. Since M_s is sufficiently small, the decrease in the exchange energy more than compensates for the increase in the magnetostatic energy, resulting in an energetically more favorable Néel wall.

III. WALL MOTION UNDER EASY AXIS FIELD

A detailed study of wall motion requires solutions of the Landau-Lifshitz equation of motion at each spatial mesh point:

$$\frac{d\mathbf{M}}{dt} = \gamma(\mathbf{M} \times \mathbf{H}_{\text{eff}}) - \frac{\lambda}{M_s} \mathbf{M} \times (\mathbf{M} \times \mathbf{H}_{\text{eff}}), \quad (3)$$

where $\gamma = -1.76 \times 10^7$ Oe⁻¹ sec⁻¹ is the gyromagnetic ratio, \mathbf{H}_{eff} can be obtained from Eq. (2), and the damping parameter λ is related to the dimensionless damping constant α by the relation $\lambda = |\gamma| \alpha$. For simplicity we shall denote the absolute value of gyromagnetic ratio by γ alone.

Applying a uniform field in the z direction to the equi-

TABLE I. Total and component energies in erg cm⁻² for asymmetric Bloch domain walls in a 1000-Å film at various values of saturation magnetization M_s . Also shown is Aharoni's self-consistency parameter S for this model.

M_s (emu cm ⁻³)	γ_{ex}	γ_{an}	γ_{mag}	γ_{tot}	S
200	0.4777	0.0091	0.6430	1.1298	1.0043
300	1.3393	0.0057	0.2592	1.6042	1.0004
400	1.5154	0.0058	0.2194	1.7406	1.0002
600	1.6900	0.0059	0.2168	1.9127	1.0007
800	1.7804	0.0060	0.2591	2.0454	1.0003
1200	1.8941	0.0060	0.4228	2.3229	1.0013
1600	2.0900	0.0061	0.4926	2.5887	1.0015

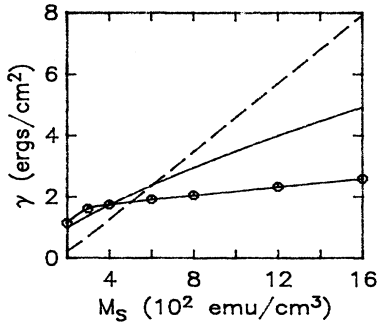


FIG. 2. Wall energy per unit area vs saturation magnetization in a 1000-Å-thick film, with the same parameters as Permalloy except M_s . Solid, dashed lines, and circles correspond to Bloch, Néel walls in 1D approximation, and 2D simulation result, respectively.

librium wall obtained above, a dynamic algorithm²⁵ is utilized to follow the detailed time evolution of the wall by a comoving coordinate system. The center of the domain wall is defined to be the x position where the magnetization component along the field direction is closest to zero. After each time step of the integration of Eq. (3), the magnetization distribution is updated by moving the wall center to the center point of the discretization region. The spins at the right and left ends of the discretization region are always assumed to be parallel to the two opposite domain directions, while the magnetizations at the film surfaces are set free.⁵ Distance and time have been scaled to the discretization cell size and gyromagnetic ratio γ , respectively.

For typical Permalloy thin films thinner than about 2000 Å, wall dynamics is mainly determined by spin relaxation effects.²⁶ Since all our simulated materials fall within this category, in the discussions below, the eddy current damping will be neglected, and the intrinsic damping constant is assumed to be 0.02 (Ref. 26) unless otherwise stated.

A. Steady-state motion

For a sufficiently small applied field, uniform wall motion is observed. The single vortex keeps its identity just as for subcritical one-dimensional wall motion.²⁵ The wall configurations at any time after the field is applied look virtually the same as in Fig. 1.

If the wall does not change its configuration during

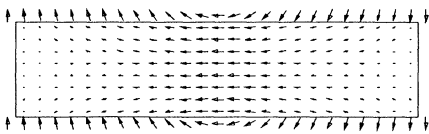


FIG. 3. Néel wall structure in a 1000-Å-thick film with $M_s = 200$ emu cm $^{-3}$. Arrows inside the frame show x - y projections of magnetization; top and bottom vectors show the x - z projections of the upper and lower film surface magnetizations.

motion, an equivalent damped mechanical oscillator²⁶⁻²⁸ representation can be used:

$$m \frac{d^2x}{dt^2} + \beta \frac{dx}{dt} + 2M_s H_c = 2M_s H_0. \quad (4)$$

Here H_0 is the applied field in z direction, x is the wall center coordinate, and H_c is the coercivity for wall motion under an easy-axis field. An effective mass m and viscosity coefficient β per unit wall area may be associated with the wall. As a practical application, they are utilized to characterize high-frequency magnetic recording head performance²⁸ and usually a one-dimensional model of domain wall motion is still used in obtaining estimates of these values micromagnetically. Using Néel's simplification²⁹ for treating wall energy in finite-thickness films, one can obtain analytical results for the wall energy, thickness,⁴ and wall mass.³⁰ For such a one-dimensional domain wall, the mass and the viscosity are as follows:

$$m = \frac{1}{N\gamma^2} \frac{\gamma_{ex}}{A}, \quad (5)$$

$$\beta = \frac{M_s \alpha}{\gamma} \frac{\gamma_{ex}}{A}, \quad (6)$$

where γ_{ex} is the exchange energy per unit area and N the effective demagnetizing factor.³⁰ The derivation and explicit result for thin films are included in Appendix B. For bulk material or infinitely thin film, the above formulas can be simplified to

$$m = \frac{1}{4\pi\gamma^2} \frac{\gamma_w}{2A}, \quad (7)$$

$$\beta = \frac{M_s \alpha}{\gamma} \frac{\gamma_w}{2A}, \quad (8)$$

where $\gamma_w = 4(AK)^{1/2}$ is the total wall energy per unit area in bulk material. For Permalloy material, and with a damping constant 0.02, these values are

$$m(\text{bulk}) = 1.63 \times 10^{-11} \text{ g cm}^{-2},$$

$$\beta(\text{bulk}) = 0.058 \text{ g cm}^{-2} \text{ sec}^{-1}.$$

It is one of our motivations in this work to examine the validity of this approach from a direct two-dimensional simulation. These simplified approximations serve as a comparison to the true values of mass and viscosity (or mobility as well) obtained below.

For a two-dimensional wall, the time for the velocity to saturate and the magnitude of the final stable velocity were obtained from numerical simulation, and compared to the formulas derived from the harmonic oscillator approximation Eq. (4):

$$\tau = \frac{m}{\beta}, \quad (9)$$

$$v = \frac{2M_s H_0}{\beta}. \quad (10)$$

Equations (9) and (10) were then utilized to solve for m and β . For $H_0 = 10$ Oe, these values are shown in Fig. 4

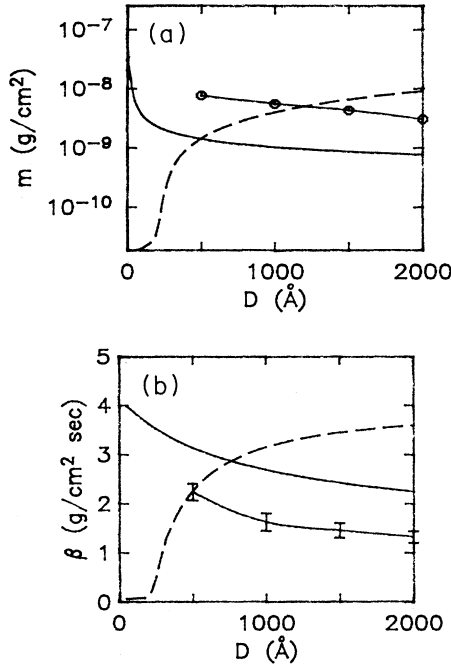


FIG. 4. (a) Wall mass per unit area vs film thickness for Permalloy; (b) wall viscosity coefficient per unit area vs film thickness. Solid, dashed lines, and circles correspond to Bloch, Néel walls in 1D approximation, and 2D simulation result, respectively.

in comparison to the results from the 1D approximation obtained from Eqs. (5) and (6). It is clear that they do not agree with each other. This implies that the mechanism for 1D wall motion (see discussion in Appendix B) may not be valid at all, and a full two-dimensional model has to be taken into account for wall dynamics. The simulation results are about 2 orders of magnitude larger than the bulk value. The two-dimensional wall is much more massive, indicating extra wall inertia mainly due to the vortex structure, or in other words, due to the magnetostatic interaction caused by finite film thickness. The presence of the film thickness makes it energetically favorable to avoid surface poles by closing the magnetic flux path inside the film, hence giving rise to a single vortex structure. This tendency to keep a flux-closure vortex yields substantial inertia when the wall is moving. The flux-closure structure also forces the spins to reverse their direction completely over a distance smaller than the film thickness, thus giving rise to a substantial amount of ex-

change stiffness, which in turn causes the viscosity coefficient to be much larger than the bulk value.

A comparison of a previous variational result on wall dynamics¹⁶ and our simulation is listed in Table II. It is seen that the mass obtained from a Ritz model is only about four times greater than the bulk value, and still 2 orders of magnitude smaller than the direct simulation results. It is also noted that the wall mobility,

$$G = \frac{v}{H_0} = \frac{2M_s}{\beta} \quad (11)$$

obtained in our simulation falls within the right order of magnitude established from experiments.^{15,26} However, it is known that even in one-dimensional Bloch wall motion, the wall mobility is nonlinearly decreasing as the applied field increases. An analytical solution of the Landau-Lifshitz equation (3) by Walker³ yields a much more reduced velocity than one would predict using the linear mobility from Eqs. (8) and (11). The dependence of wall velocity on external fields below the Walker limit field $H_w = \alpha 2\pi M_s$ (Refs. 3 and 31) (which is 100 Oe in this case) for both our simulation and the 1D rigorous solution is shown in Fig. 5. The maximum wall velocity in the thin film is much smaller than that predicted from even rigorous one-dimensional considerations.³¹ In thin films one can observe the same nonlinearly decreasing mobility, only now it is smaller by less than an order of magnitude than the 1D result.

B. High-field dynamics

For an easy-direction field much larger than the anisotropy field $H_k = 2K/M_s = 2.5$ Oe, we have observed wall dynamics similar to the 1D case.²⁵ For fields higher than 40 to 60 Oe, the thin film wall velocities shown in Fig. 5 are not steady values, but averaged over many integration points. The wall velocities fluctuate or even oscillate, due to the fact that wall structure transitions are induced in the high-field region.

For a 500-Å-thick Permalloy film, a typical velocity evolution under high field is shown in Fig. 6. For $H_0 = 80$ Oe, the wall velocity oscillates periodically while the net average is along the normal motion direction. This periodic wall motion is more complex than, but bears resemblance to, the supercritical motion in a one-dimensional wall.^{25,31,32} In one dimension, when the applied field exceeds the Walker limit field, the original Bloch wall rotates around its forward motion direction, changes into a Néel wall, then to a Bloch wall and a Néel wall with opposite chiralities, and finally resumes the

TABLE II. Comparison of various wall energy terms and wall masses per unit area for a 1000-Å-Permalloy film. Case 1, Aharoni's Ritz model result was obtained by minimizing the wall Lagrangian function at $v = 100$ m/sec; case 2, numerical simulation was for the case of $\alpha = 0.02$ and $H_z = 10$ Oe.

Case	v (m/sec)	γ_{ex} (erg cm ⁻²)	γ_{an} (10 ⁻³ erg cm ⁻²)	γ_{mag} (erg cm ⁻²)	γ_{tot} (erg cm ⁻²)	m (10 ⁻¹¹ g cm ⁻²)
1	100	2.3406	5.1697	0.1653	2.5182	7.1
2	99	1.8273	5.7064	0.2822	2.1292	550.0

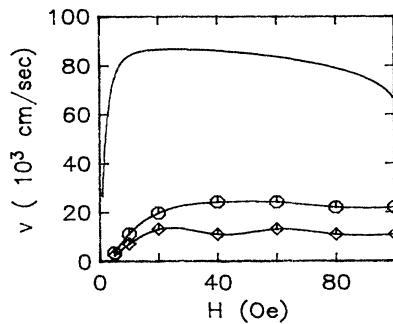


FIG. 5. Wall velocity vs applied field in easy direction for Permalloy. Solid line, 1D analytic solution; circles, 1000-Å thick film; diamonds, 500-Å thick film.

original wall structure. Such a periodic motion occurs because the applied field is sufficient to break the torque balance with the demagnetization field which is essential in maintaining a steady state. In a 500-Å-thin film, a similar process takes place. The magnetization configurations at circled points in Fig. 6 are shown successively in Figs. 7(a)–7(g). As time increases, the originally counterclockwise winding vortex wall [Fig. 7(a)] is driven out of the lower film surface [Fig. 7(b)], later forming an asymmetric Néel wall with central spins pointing up [Fig. 7(c)]. After the emergence of a Néel wall with most of the central spins pointing in plane toward the wall motion direction [Fig. 7(d)], another similar asymmetric Néel wall with central spins pointing down [Fig. 7(e)] is created. It then evolves into almost a clockwise winding single vortex emerging from the top surface of the film [Fig. 7(f)]. The half period of this oscillation is completed by the formation of a complete vortex wall [Fig. 7(g)] in the film center with opposite flux-closure rotation to the original one. The oscillatory transition between Bloch and Néel wall manifests itself by the oscillation of wall velocity (Fig. 6), since the masses and viscosities of these two walls are very different from each other (Fig. 4). One can follow the rotation of the central spin (the magnetization which has the largest component in the cross-sectional plane) driven gyromagnetically by the applied field in the z direction as a guide to the dynamic

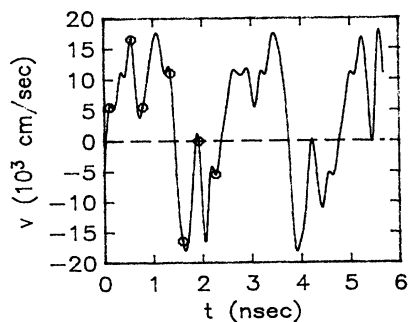


FIG. 6. Wall velocity vs time for a 500-Å-thick Permalloy film. $H_0 = 80$ Oe is applied in z direction at $t = 0$.

series shown above.

For a 2000-Å film, a different dynamic evolution of wall structures is shown in Figs. 8(a)–8(d). The single vortex [Fig. 8(a)] elongates first [Fig. 8(b)], then develops out-of-plane magnetization at the upper film surface, forms a frontal vortex in the center [Fig. 8(c)], and finally breaks into three flux-closure vortices with different sizes and chiralities [Fig. 8(d)]. The oscillatory transition be-

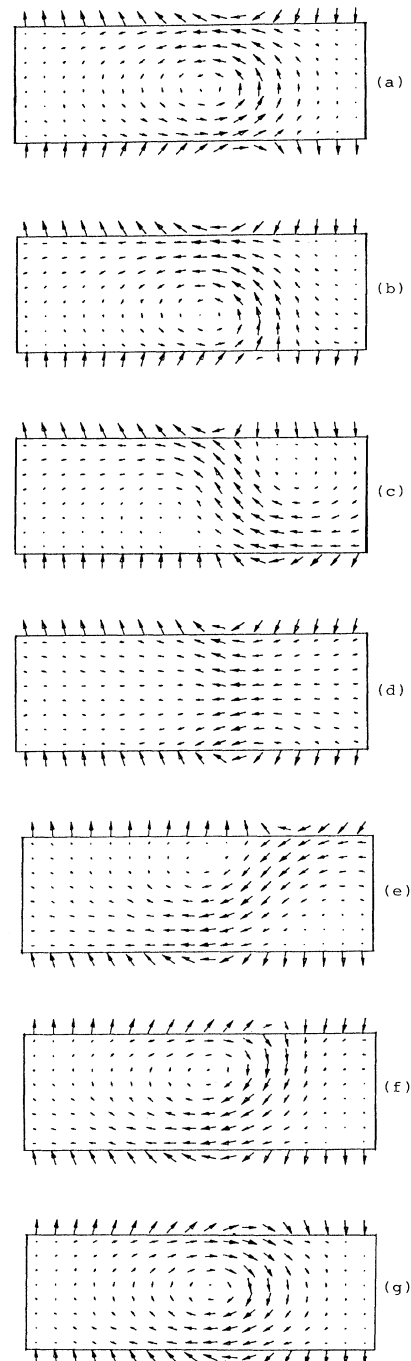


FIG. 7. Wall configurations at circled times in Figs. 8(a)–8(g). The vector plots have the same notation as in Fig. 5.

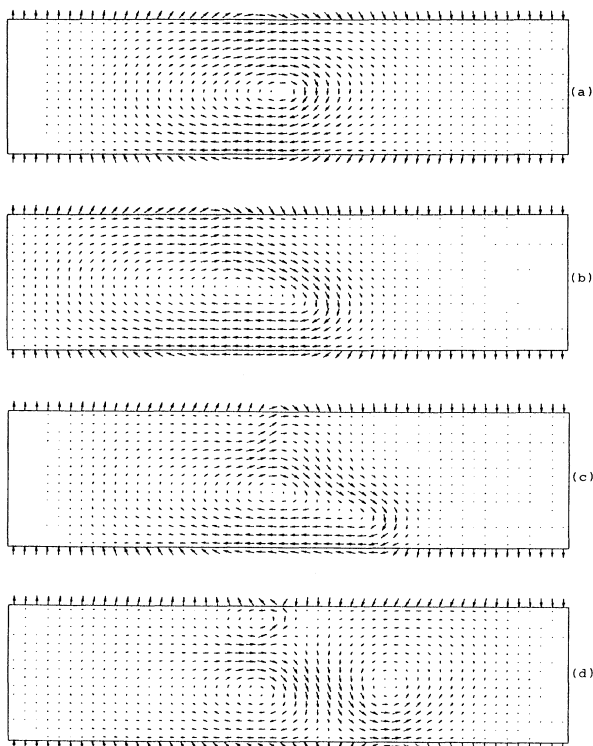


FIG. 8. Wall configurations of a 2000-Å-thick Permalloy film, after 80 Oe easy-axis field is applied. (a) $t=0.11$ nsec; (b) $t=0.34$ nsec; (c) $t=0.68$ nsec; (d) $t=1.25$ nsec.

tween Bloch and Néel walls as seen in the 500-Å film is not realized here, since the film thickness is large enough to accommodate multiple vortices, and also to make the Néel wall energetically less favorable than in the thinner film. For films of other thicknesses, this break-up of a single vortex is typical. For example, in a 1000-Å-thick film, the single vortex breaks into two vortices and then changes to another single vortex with opposite chirality at $H_0=80$ Oe (similar phenomenon has been observed for $H_0=200$ Oe at a larger damping $\alpha=0.1$).³³ Therefore, the evolution of a single vortex into multivortices serves as a precursor for more complicated nonlinear behavior as the applied field increases. For even higher applied fields, turbulent behavior of the wall motion is observed, hence verifying that, in agreement with previous claims,^{25,34,35} the wall motion under high field is prone to chaotic instability.

IV. WALL STRUCTURE TRANSITIONS UNDER HARD-AXIS FIELD

With an external field applied in the hard direction and in the film plane, the asymmetric Bloch wall will gradually change to a Néel wall as the field increases. This transition is expected since when $H_x \geq H_k$, all the magnetizations in the domain and wall region will be saturated in the x direction. Therefore at some point along the way, the energy of a Néel wall will be lower than that of a Bloch wall.^{7,36} Similarly, a transition from a Néel to a

Bloch wall is expected when the field is reduced from saturation to zero.

Since surface charges exist at the left and right ends of the discretization region, the magnetostatic energy of the wall cannot be separated from that of the domains,³⁷ and a slightly different formulation of the demagnetizing field in Eq. (2) is required. The wall region is extended into semi-infinite left and right single domains, whose dynamics are determined by their corresponding Landau-Lifshitz equations. Since the domain magnetization is close to that of the adjacent column of prisms, the net magnetic surface charges at the left and right edges of the discretization region are almost canceled.^{21,22} The magnetostatic interaction of the wall and the domains is thus taken into account simultaneously. This modified demagnetizing field formulation is also included in Appendix A.

Simulating a hysteresis loop, a spatially uniform external field is applied along the x direction and varied stepwise from a positive saturation field value ($H_x \geq H_k$) to the negative, and then back to the positive value again. A modified energy minimization iteration³⁸ is used to obtain stable equilibrium states. At each field step, the applied field H_x was kept constant until an equilibrium distribution was obtained.³⁹ All iterations have been carried out until the maximum difference between magnetization vectors obtained from two successive iterations is within an error of 1×10^{-7} . Also, additional perturbations are applied to each iterated final state in order to obtain stable equilibrium.^{38,39} If the perturbed magnetization orientations evolve back to the initially obtained configuration, then the equilibrium configuration is accepted and the iteration proceeds. It is seen that having too small a convergency criterion (as small as 1×10^{-4} sometimes) and not perturbing the premature iterations would lead to a metastable intermediate state which could be falsely identified as a true energy minimum.

For hard-axis driving fields, the hysteresis loop is a straight line without hysteresis according to single domain theory.^{40,41} However, in our simulations constricted hard axis loops are obtained. The magnetization component along the applied field direction versus field value is plotted in Fig. 9 for Permalloy films with 500- and 1000-Å thicknesses. The loops are seen to open up within certain ranges of the applied field. A series of the wall structures in a 500-Å film is shown in Fig. 10 as H_x is decreased from 2.5 Oe (the anisotropy field) to -2.5 Oe (only structures between field values 1.25 Oe and -1.25 Oe are shown). Starting from full saturation in the x direction, the wall takes a form of an asymmetric Néel wall [Fig. 10(a)] as the applied field is decreased. The central spins point in the film normal direction, hence producing two oppositely winding vortices on both sides [Fig. 10(b)]. At a critical external field this structure abruptly changes into an asymmetric Bloch wall [Fig. 10(c)]. With increasing field in the opposite direction, the single vortex is driven up toward the film surface; at another critical field H_{BN} , this single vortex annihilates against the surface [Fig. 10(d)] and an asymmetric Néel wall with central spins pointing toward the opposite direction to that shown in Fig. 10(a) is created [Fig. 10(e)]. Such a series completes one half of the hysteresis

loop, while the other half is completed by going from Fig. 10(a) to 10(e), with all the magnetizations exactly opposite to those shown before. Such configurations are energetically degenerate with the previous ones, and the alternate transitions between these structures generate the complete loop.

Thus, irreversible hysteretic wall-structure transitions have been observed under a slowly varying hard-axis field. This hysteresis is due to the asymmetry of internal structural changes of the domain walls, rather than other simpler mechanisms proposed for constricted hard-axis loops.^{23,42} The two critical fields for the irreversible transitions H_{NB} and H_{BN} do not have the same value and are plotted in Fig. 11. It is seen that, starting from the remanent state (asymmetric Bloch wall) and starting from the saturation state (Néel wall), we have different critical fields corresponding to the two different transition patterns depicted in Figs. 10(b) and 10(d). The critical field for the Bloch-Néel wall transition H_{BN} increases with increasing film thickness, which is in agreement with the fact that Néel walls are favored in thinner films while Bloch walls are favored in thicker films, hence it becomes more difficult for the Bloch to Néel wall transition to occur for thicker films. Similarly, the other transition field H_{NB} also increases with increasing film thickness.

The Landau-Lifshitz equation (3) is also solved to study the transition behavior. For a field larger than the transition field H_{BN} , starting from a 180° asymmetric Bloch wall (remanent state), a series of wall structures similar to those shown from Figs. 10(c)–10(e) (Ref. 33) are obtained (notice the reverse order); similarly, starting with a symmetric Néel wall (saturation state), for a field

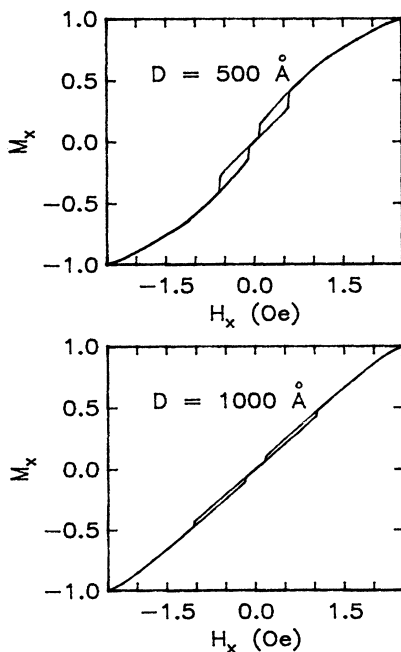


FIG. 9. Constricted hard-axis hysteresis loops for Permalloy films with 500 and 1000 Å thicknesses.

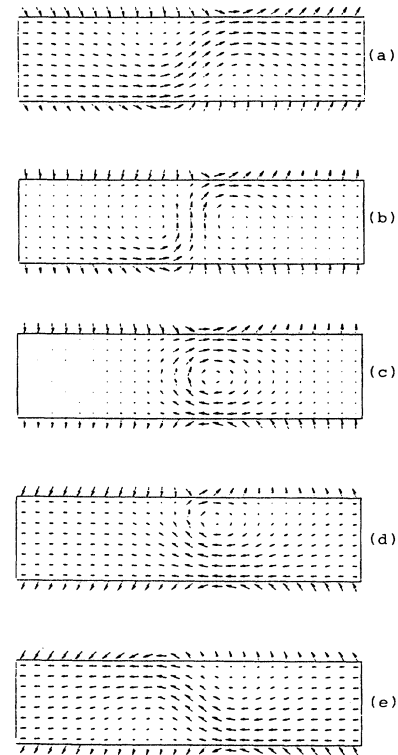


FIG. 10. Wall-structure transitions under varying hard direction field in a 500-Å Permalloy film. (a) $H_x = 1.25$ Oe; (b) $H_x = 0.25$ Oe; (c) $H_x = 0.0$ Oe; (d) $H_x = -1.0$ Oe; (e) $H_x = -1.25$ Oe.

smaller than the transition field H_{NB} , the dynamic wall-structure evolution closely resembles that shown in Figs. 10(a)–10(c). However, here the variable is time instead of field magnitude.

This transition is similar to one of the mechanisms in explaining wall-creep phenomena.¹⁷ When a domain wall in a thin film is driven by an easy-axis field, the application of a hard-axis bias field will change the wall structure. Since the masses and viscosities of the Bloch and Néel walls are different, the dynamic behavior of the wall will be changed accordingly. This effect had been confirmed by experiments,^{18,43–45} but given many different explanations to its mechanism.⁴⁶ The critical

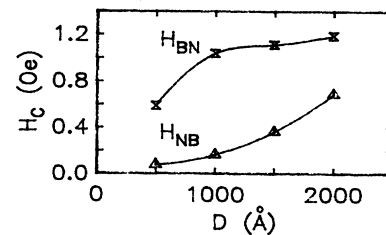


FIG. 11. Hard direction critical fields for wall-structure transitions vs film thickness for Permalloy. Hourglasses (upper curve) represent H_{BN} ; triangles (lower curve) represent H_{NB} .

fields for the Bloch-Néel transition H_{BN} (upper curve in Fig. 11) assume values from $0.24H_k$ to $0.48H_k$, which agree with data from wall-creep experiments.^{17,43} In low-frequency wall-creep experiments,⁴⁵ an abrupt wall motion occurs during a high field ($0.4H_k$) and a low field ($0.1H_k$) transition by the hard-axis field. These fields also fall within our calculated values of H_{BN} and H_{NB} . The hysteretic transitions we have observed in this study could be experimentally inferred by adding an oscillating hard-axis bias field. During different half cycles of the bias period, since the intermediate walls have drastically different configurations, it is expected that the wall mobility would change correspondingly. Hence, a direct observation of the time dependence of wall motion correlated with the ac hard-axis field should confirm this effect. However, better Kerr optical observation on dynamic wall configurations directly is the best way to determine this.

V. CONCLUSION

Realistic wall structures in thin film exhibit two-dimensional characteristics. The most prominent feature compared to a one-dimensional wall is the magnetostatically favored flux-closure vortex. This gives rise to extra wall inertia, resulting in an effective wall mass and viscosity typically 2 orders of magnitude larger than a 1D wall in bulk material. For an applied field in the easy axis direction, wall motion is uniform for small fields, but starts to create extra vortices and show turbulent behavior at fields much higher than the anisotropy field; for thinner films, oscillatory behavior of the wall-structure transition is possible. For an increasing applied field in the inplane hard direction, the original single vortex is annihilated at the film surface and two half vortices are created in the film center. The wall structure changes from an asymmetric Bloch wall to a Néel wall. Starting from a saturated Néel wall and decreasing the hard-axis field, a different wall transition pattern is observed. Two complete vortices are created; one of them is subsequently annihilated to yield the single vortex asymmetric Bloch wall. This irreversible structural transition offers an alternative mechanism to wall-creep phenomena.

ACKNOWLEDGMENTS

This research was supported by the Center for Magnetic Recording Research at UCSD, and by the National Science Foundation under Grant No. NMR-87-07421. The authors would also like to thank the San Diego Supercomputer Center for providing a Grant to perform these studies on the Cray Y-MP supercomputer.

APPENDIX A: SIMPLE FORMULATION OF MAGNETOSTATIC INTERACTION IN THIN FILMS

For the purpose of evaluating the contributions of the magnetostatic interactions to the equilibrium and dynamics of a domain wall, one usually starts with some form of demagnetizing energy.^{5,13,21,22} In this appendix, however, we show a simple derivation of this contribution, utilizing the demagnetizing field directly.

For a two-dimensional magnetization configuration without a z dependence, the demagnetizing field can be expressed as

$$\mathbf{H}(\mathbf{r}) = -2 \int_A d^2r' \frac{\nabla' \cdot \mathbf{M}'(\mathbf{r}-\mathbf{r}')}{|\mathbf{r}-\mathbf{r}'|^2} + 2 \int_C dl' \frac{\hat{\mathbf{n}}' \cdot \mathbf{M}'(\mathbf{r}-\mathbf{r}')}{|\mathbf{r}-\mathbf{r}'|^2}, \quad (\text{A1})$$

where \mathbf{r} is the polar vector in the plane perpendicular to z , and the integrations are over the area A and the boundary circumference C . For a constant magnetization, only the surface charge term remains in Eq. (A1):

$$\mathbf{H} = 2 \int dl' \frac{\sigma(\mathbf{r}-\mathbf{r}')}{|\mathbf{r}-\mathbf{r}'|}, \quad (\text{A2})$$

in which $\sigma = \mathbf{M} \cdot \hat{\mathbf{n}}$ is the surface charge density. The two demagnetizing field components can be easily evaluated from Eq. (A2):

$$H_x = -2\sigma(\theta_2 - \theta_1), \quad (\text{A3})$$

$$H_y = -2\sigma \ln \left[\frac{r_2}{r_1} \right], \quad (\text{A4})$$

where r and the θ 's are the radii and polar angles of the two bounding vectors shown in Fig. 12. H_x and H_y are the demagnetizing field components normal and tangential to the surface pole density distribution, respectively. The direction of the demagnetizing field is always away from the positive surface charges and toward the negative charges.

Given the above basic formulation, one can proceed to calculate the demagnetizing fields arising from the four sides of a discretization prism. The magnetization inside each prism is assumed to be constant and only the surface charges on its four sides contribute to the magnetostatic energy.⁵ Adding up the demagnetizing fields acting on prism (i, j) by all the other different prisms (i', j') in the discretization region, we have, for the interacting field on the site (i, j)

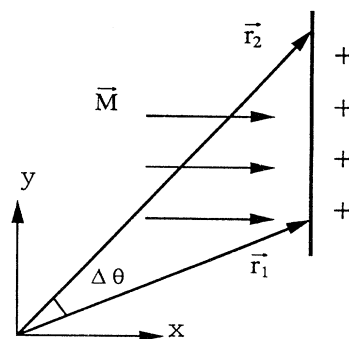


FIG. 12. The coordinate system for evaluating the demagnetizing field due to a constant two-dimensional magnetization.

$$\mathbf{H}(i,j) = \sum_{i'=1}^{N_x} \sum_{j'=1}^{N_y} M_s \left\{ [m_x(i',j')B(k,l) + m_y(i',j')C(k,l)]\hat{\mathbf{x}} + [m_x(i',j')C(k,l) - m_y(i',j')B(k,l)]\hat{\mathbf{y}} \right\}, \quad (\text{A5})$$

in which $\mathbf{m} = \mathbf{M}/M_s$ is the unit vector in the direction of the local magnetization, the indices are $k = i' - i, l = j' - j$, and the coefficients B and C are defined as follows:

$$B(k,l) = B_1(k,l) + B_2(k,l),$$

$$C(k,l) = C_1(k,l) + C_2(k,l),$$

$$B_1(k,l) = -g_1(k+1, l+1) + g_1(k+1, l), \quad (\text{A6a})$$

$$C_1(k,l) = -g_2(k+1, l+1) + g_2(k+1, l), \quad (\text{A6b})$$

$$B_2(k,l) = g_1(k, l+1) - g_1(k, l), \quad (\text{A6c})$$

$$C_2(k,l) = g_2(k, l+1) - g_2(k, l). \quad (\text{A6d})$$

The intrinsic functions used above are

$$g_1(i,j) = 2 \tan^{-1} \left[\frac{j - \frac{1}{2}}{i - \frac{1}{2}} \right],$$

$$g_2(i,j) = \ln \left[\left(i - \frac{1}{2} \right)^2 + \left(j - \frac{1}{2} \right)^2 \right].$$

It is easier to formulate the self-magnetostatic energy of each prism separately⁵ and set $B(0,0) = C(0,0) = 0$. Then one can use Eq. (A5) to evaluate the interaction demag-

netizing field at each prism and equate $-\frac{1}{2}\mathbf{H}(i,j) \cdot \mathbf{M}(i,j)$ to the magnetostatic interaction energy density at that point. Adding this to the self-energy and summing over the whole discretization region would thus yield the total magnetostatic energy.

For domain walls under a hard-axis applied field, 180° walls would no longer exist in general. The magnetostatic energy of the wall cannot be considered separately from that of the surrounding domains.³⁷ The discretization region ends with a charge on the surfaces of the left-most and right-most columns of prisms. In order to eliminate this discretization effect, semi-infinite domain regions with constant magnetizations are assumed, and the domain surface charge terms are included in the magnetostatic interaction field with each prism inside the discretization region. Due to the large demagnetizing factor from the thin film surfaces, the magnetizations in the domains are practically always in the film plane, and only M_x contribute to the magnetostatic interactions with the wall.

The columns $i=0$ and $i=N_x+1$ correspond to the surfaces of the left and right domains, respectively. The interaction field on prism (i,j) due to the domain charge densities on these two columns can be expressed as

$$\begin{aligned} \mathbf{H}_{\text{domain}}(i,j) = -M_s \sum_{i'=1}^{N_x} \sum_{j'=1}^{N_y} [m_x(0,j')B_2(1-i, j'-j) + m_x(N_x+1, j')B_1(N_x-i, j'-j) \\ + m_x(0,j')C_2(1-i, j'-j) + m_x(N_x+1, j')C_1(N_x-i, j'-j)], \end{aligned} \quad (\text{A7})$$

where the coefficients $B_1, B_2, C_1,$ and C_2 's are already defined in Eqs. (A6). Adding Eq. (A7) to Eq. (A5) effectively nearly cancels the net surface charges at the edges of the discretization region^{21,22,37} and gives the proper magnetostatic interactions.

APPENDIX B: ANALYTIC APPROXIMATIONS TO DOMAIN WALL MASS AND VISCOSITY

In this appendix we will discuss some approximation models of domain walls in thin films in order to obtain order of magnitude estimates of wall mass and viscosity. The simplest one²⁹ assumes that the magnetization is only one dimensional. For extremely thick films, this is the actual case which yields the bulk-material results; for extremely thin films, the free boundary conditions on the film surfaces⁵ $\partial \hat{n} / \partial y = 0$ suppresses the y dependence of \mathbf{M} so that the above statement is also true. For films of intermediate thickness, this approximation allows the Bloch and Néel wall as two possible wall structures so

that one can obtain their structural parameters through an energy variational method.

Assuming that the wall velocity is small enough so that the wall does not change its static configuration very much, one can derive the expressions for a 1D wall's mass and viscosity. Under an applied field H_0 in the easy axis (z direction), M_x in Bloch wall and M_y in Néel wall causes the demagnetizing field H_e .³⁰ The spins in the wall precess about H_e at Larmor frequency in a sense which opposes any change in the motion of a wall hence give rise to an effective wall inertia.² The demagnetizing field is

$$H_e = \frac{1}{\gamma} \frac{\partial \theta}{\partial t} = -\frac{v}{\gamma} \frac{\partial \theta}{\partial x} \quad (\text{B1})$$

and is related to the magnetizations by

$$H_e = -NM_n. \quad (\text{B2})$$

The demagnetizing factor N and the normal component

of the magnetization M_n which causes the demagnetizing field are

$$M_n = \begin{cases} M_x & \text{Bloch wall,} \\ M_y & \text{Néel wall,} \end{cases} \quad (\text{B3a})$$

$$N = \begin{cases} \frac{4\pi D}{a+D} & \text{Bloch wall,} \\ \frac{4\pi a}{a+D} & \text{Néel wall,} \end{cases} \quad (\text{B3b})$$

where a is the wall width and D is the film thickness.

The energy associated with the demagnetizing field H_e is

$$\begin{aligned} E &= -\frac{1}{2} \int (M_n \cdot H_e) dV = -\frac{1}{2N} \int H_e^2 dV \\ &= \frac{v^2 S}{2N\gamma^2} \int_{-\infty}^{\infty} \left(\frac{\partial \theta}{\partial x} \right)^2 dx, \end{aligned} \quad (\text{B4})$$

where S is the wall area perpendicular to the wall motion direction. Equating the above expression to the kinetic energy $\frac{1}{2}mv^2$, one obtains the wall mass per unit area:

$$m = \frac{1}{N\gamma^2} \int_{-\infty}^{\infty} \left(\frac{\partial \theta}{\partial x} \right)^2 dx = \frac{1}{N\gamma^2} \frac{\gamma_{\text{ex}}}{A}, \quad (\text{B5})$$

which is Eq. (5).

Since \mathbf{H}_0 , \mathbf{H}_e , and \mathbf{M} are perpendicular to each other at the wall center, and $\mathbf{H} = \mathbf{H}_0 + \mathbf{H}_e$, the power dissipated per unit volume^{2,15} is

$$\begin{aligned} \mathbf{H} \cdot \frac{d\mathbf{M}}{dt} &= -\frac{\gamma}{M_s} \mathbf{H} \cdot [(\mathbf{M} \cdot \mathbf{H})\mathbf{M} - M_s^2 \mathbf{H}] \\ &= -\frac{\gamma}{M_s} [(\mathbf{M} \cdot \mathbf{H})^2 - M_s^2 H^2] \\ &= \gamma \alpha M_s H_e^2 \end{aligned} \quad (\text{B6})$$

in which the Landau-Lifshitz equation (3) has been utilized. Equating the spatial integration of this power to $2M_s H_0 v$, one obtains

TABLE III. Wall viscosity coefficients per unit area β in $\text{g cm}^{-2} \text{sec}^{-1}$ for Permalloy film of various thicknesses. Comparison of the β 's, obtained from evaluating Eq. (B9) using equilibrium magnetization distributions (case 1), and from evaluating Eq. (10) using dynamic simulation data at $H_z = 10$ Oe (case 2), is listed for different dampings.

α	Case	β for film thickness of		
		500 Å	1000 Å	2000 Å
0.02	1	1.63	0.84	0.49
	2	2.24	1.62	1.32
0.1	1	8.14	4.18	2.44
	2	8.95	4.85	4.04

$$2M_s H_0 v = \gamma \alpha M_s \int_{-\infty}^{\infty} H_e^2 dx = \frac{\alpha M_s v^2}{\gamma} \int_{-\infty}^{\infty} \left(\frac{\partial \theta}{\partial x} \right)^2 dx. \quad (\text{B7})$$

Using Eq. (10) the viscosity can then be easily evaluated to be

$$\beta = \frac{2M_s H_0}{v} = \frac{\alpha M_s}{\gamma} \int_{-\infty}^{\infty} \left(\frac{\partial \theta}{\partial x} \right)^2 dx = \frac{\alpha M_s}{\gamma} \frac{\gamma_{\text{ex}}}{A}, \quad (\text{B8})$$

which gives us Eq. (6).

One can also evaluate the viscosity for a two-dimensional wall using the same assumptions made above.¹⁵ The viscosity coefficient per unit wall area (in the y - z plane) is

$$\beta = \frac{M_s \alpha}{\gamma} \frac{1}{D} \int dx \int dy \left[\left(\frac{\partial \theta}{\partial x} \right)^2 + \sin^2 \theta \left(\frac{\partial \phi}{\partial x} \right)^2 \right]. \quad (\text{B9})$$

In one-dimensional approximation, this expression reduces to Eq. (B8). In Table III, reasonable agreement is shown between the direct simulation results on β and those obtained by evaluating Eq. (B9) using the equilibrium magnetization distributions of the two-dimensional walls. The discrepancy of the data is caused by the slightly changing wall configurations during the wall motion.

*Also at the Center for Magnetic Recording Research at UCSD.

¹C. Kittel, Phys. Rev. B **80**, 918 (1950).

²J. Galt, Phys. Rev. B **85**, 664 (1952).

³L. R. Walker, in *Magnetism*, edited by G. T. Rado and H. Suhl (Wiley, New York, 1963), Vol. 3, p. 450.

⁴S. Middelhoek, J. Appl. Phys. **34**, 1054 (1963).

⁵A. E. LaBonte, J. Appl. Phys. **40**, 2450 (1969).

⁶A. Hubert, Phys. Status Solidi **32**, 519 (1969).

⁷A. Hubert, Phys. Status Solidi **38**, 699 (1970).

⁸A. Aharoni, J. Appl. Phys. **46**, 908 (1975).

⁹J. P. Jakubovics, Philos. Mag. B **30**, 983 (1974).

¹⁰S. Tsukahara and H. Kawakatsu, J. Phys. Soc. Jpn. **32**, 1493 (1972).

¹¹J. N. Chapman *et al.*, J. Magn. Magn. Mater. **49**, 277 (1985).

¹²M. R. Scheinfein *et al.*, Phys. Rev. Lett. **63**, 668 (1989).

¹³M. R. Scheinfein *et al.*, Phys. Rev. B **43**, 3395 (1991).

¹⁴A. Aharoni and J. P. Jakubovics, Phys. Rev. B **43**, 1290 (1991).

¹⁵S. Höcker and A. Hubert, Int. J. Magn. **3**, 139 (1972).

¹⁶A. Aharoni, J. Appl. Phys. **47**, 3329 (1976).

¹⁷S. Middelhoek and D. Wild, IBM J. Res. Dev. **11**, 93 (1967).

¹⁸A. L. Olson and E. J. Torok, J. Appl. Phys. **36**, 1058 (1965).

¹⁹K. U. Stein and E. Feldtkeller, J. Appl. Phys. **38**, 4401 (1967).

²⁰W. F. Brown, Jr., *Micromagnetics* (Krieger, Huntington, New York, 1978).

²¹J. Miltat, A. Thiaville, and P. Trouilloud, J. Magn. Magn. Mater. **82**, 297 (1989).

²²P. Trouilloud and J. Miltat, J. Magn. Magn. Mater. **66**, 194 (1987).

²³A. Aharoni, J. Appl. Phys. **39**, 861 (1968).

- ²⁴S. Middlehoek, *Ferromagnetic Domains in Thin Ni-Fe Films* (Drukkerij Wed. G. Van Soest N. V., Amsterdam, 1961).
- ²⁵S. W. Yuan and H. N. Bertram, *J. Appl. Phys.* **69**, 5874 (1991).
- ²⁶S. Middelhoek, *IBM J. Res. Dev.* **10**, 351 (1966).
- ²⁷W. Döring, *Z. Naturforsch.* **3a**, 373 (1948).
- ²⁸N. Smith, *IEEE Trans. Magn.* **MAG-27**, 729 (1991).
- ²⁹L. Néel, *C. R. Acad. Sci.* **241**, 533 (1955).
- ³⁰M. Prutton and K. D. Leaver, *Phys. Lett.* **6**, 15 (1963).
- ³¹N. L. Schryer and L. R. Walker, *J. Appl. Phys.* **45**, 5406 (1974).
- ³²J. C. Slonczewski, *Int. J. Magn.* **2**, 85 (1972).
- ³³S. W. Yuan and H. N. Bertram, *IEEE Trans. Magn.* (to be published).
- ³⁴F. Waldner, *J. Magn. Magn. Mater.* **31-34**, 1015 (1983).
- ³⁵H. Suhl and X. Y. Zhang, *J. Appl. Phys.* **61**, 4216 (1987).
- ³⁶A. Hubert, *Theorie der Domänenwände in Geordneten Medien* (Springer-Verlag, New York, 1974).
- ³⁷A. Aharoni and J. P. Jakubovics, *IEEE Trans. Magn.* **MAG-26**, 2810 (1988).
- ³⁸M. E. Schabes and H. N. Bertram, *J. Appl. Phys.* **64**, 1347 (1988).
- ³⁹J. Zhu and H. Neal Bertram, *J. Appl. Phys.* **66**, 1291 (1989).
- ⁴⁰E. Stoner and E. Wolfarth, *Philos. Trans. R. Soc. London* **A240**, 74 (1948).
- ⁴¹S. Chikazumi, *Physics of Magnetism* (Wiley, New York, 1964).
- ⁴²S. Middelhoek, *J. Appl. Phys.* **33**, 1111 (1962).
- ⁴³M. Labrune *et al.*, *J. Magn. Magn. Mater.* **58**, 227 (1986).
- ⁴⁴H. C. Bourne, Jr., T. Kusuda, and C. Lin, *IEEE Trans. Magn.* **MAG-4**, 440 (1968).
- ⁴⁵H. C. Bourne, Jr., T. Kusuda, and C. Lin, *IEEE Trans. Magn.* **MAG-5**, 247 (1969).
- ⁴⁶W. Kayser, *IEEE Trans. Magn.* **MAG-3**, 141 (1967).